Supporting Information

# Thermally Robust and Strongly Oxidizing Surface of $WO_3$ Hydrate Nanowires for Electrical Aldehyde Sensing with Long-Term Stability

*Guozhu Zhang,[1,2] Takuro Hosomi,[1,3] Wataru Mizukami,[3,4,5] Jiangyang Liu,[1,2] Kazuki Nagashima,[1,3] Tsunaki Takahashi,[1,3] Masaki Kanai,[1,2] Takeharu Sugiyama,[6] Takao Yasui,[3,7] Yuriko Aoki,[2] Yoshinobu Baba,[7] Johnny C Ho,[2,8] and Takeshi Yanagida[1,2*]*

[1] *Department of Applied Chemistry, Graduate School of Engineering, The University of Tokyo, 7-3-1, Hongo, Bunkyo-ku, Tokyo, 113-8654, Japan*

[2] *Institute for Materials Chemistry and Engineering, Kyushu University, 6-1 Kasuga-Koen, Kasuga, Fukuoka, 816-8580, Japan*

[3] *JST-PRESTO, 4-1-8 Honcho, Kawaguchi, Saitama 332-0012, Japan*

[4] *Center for Quantum Information and Quantum Biology, Institute for Open and Transdisciplinary Research Initiatives, Osaka University, Osaka 560-8531, Japan*

[5] *Graduate School of Engineering Science, Osaka University, 1-3 Machikaneyama, Toyonaka, Osaka 560-8531, Japan.*

[6] *Research Center for Synchrotron Light Applications, Kyushu University, 6-1 Kasuga-koen, Kasuga, Fukuoka 816-8580, Japan*

[7] *Graduate School of Engineering, Nagoya University, Furo-cho, Chikusa-ku, Nagoya 464-8603, Japan*

[8] *Department of Materials Science and Engineering, State Key Laboratory of Terahertz and Millimeter Waves, and Centre for Functional Photonics, City University of Hong Kong, Kowloon 999077, Hong Kong SAR*

[*] *Corresponding Author: Takeshi Yanagida* (*yanagida@g.ecc.u-tokyo.ac.jp)*

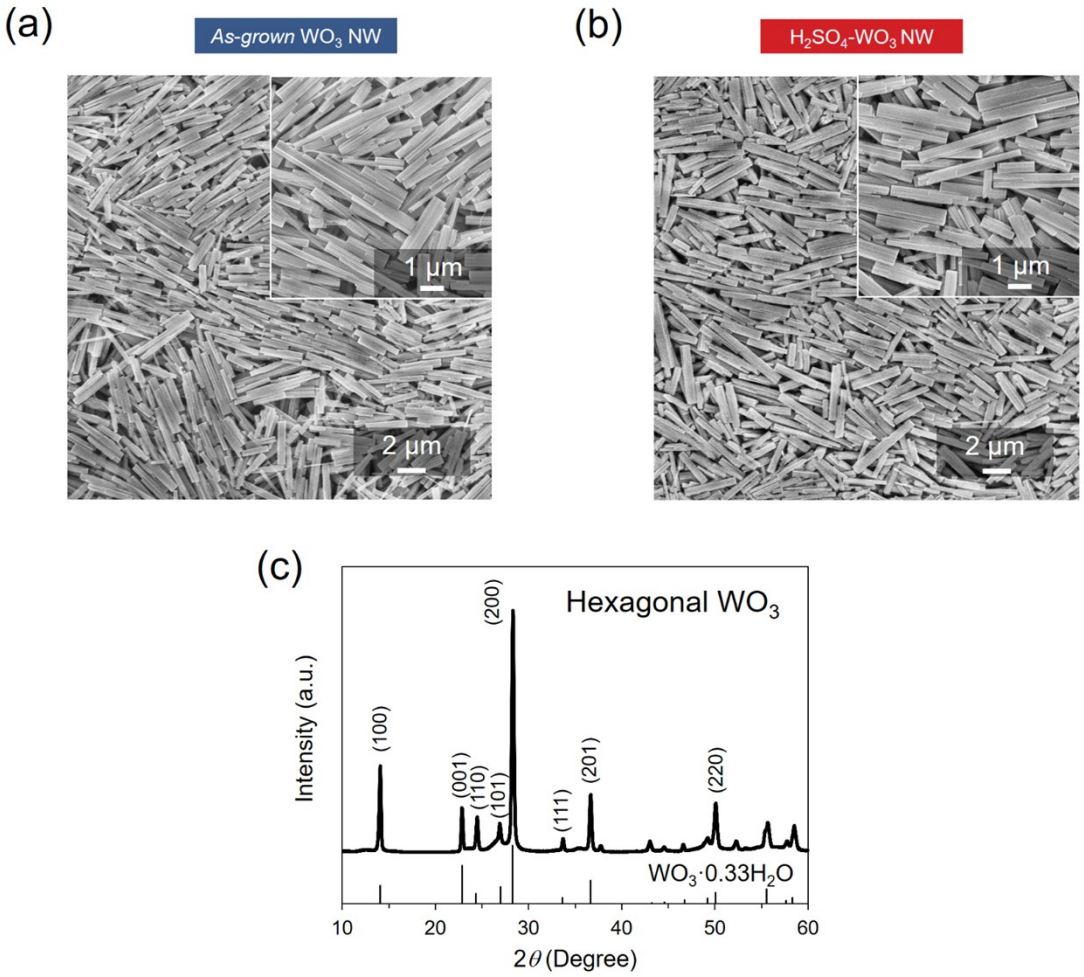


**Figure S1**. SEM image of (a) a*s-grown* and (b) $H_2SO_4$-surface treated $WO_3$ hydrate nanowire. (c) XRD pattern of *as-grown* $WO_3$ hydrate nanowire.

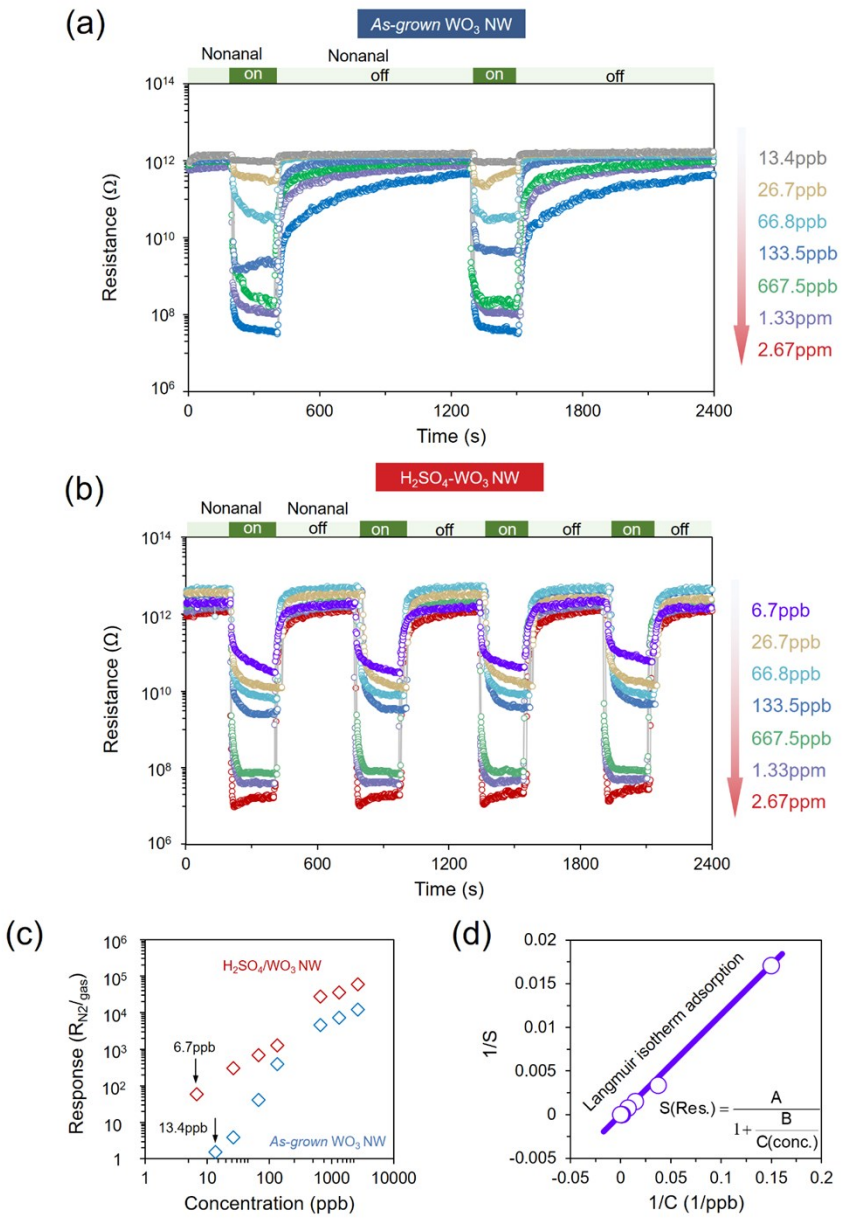


**Figure S2**. (a) and (b) Dynamic resistance response of As-grown and $H_2SO_4$-surface treated $WO_3$ nanowire sensor devices to various concentration (from 6.7 ppb to 2.67 ppm) of nonanal at 200 °C. (c) Sensing response extracted from (a) and (b). (d) Fitting of 1/*S* (reciprocal of sensor response) vs. 1/*C* (reciprocal of nonanal concentration) for $H_2SO_4$-surface treated $WO_3$ nanowire sensor devices.

The linear fitting of 1/*S* vs. 1/*C* has shown that the surface coverage of adsorbed molecules follows Langmuir isotherm. This suggests that the conductance change of the sensor device is related to the surface occupancy of the nonanal molecules binding on $WO_3$ nanowire surface, and the effect of electrode-nanowire contact is tiny. [1-3]

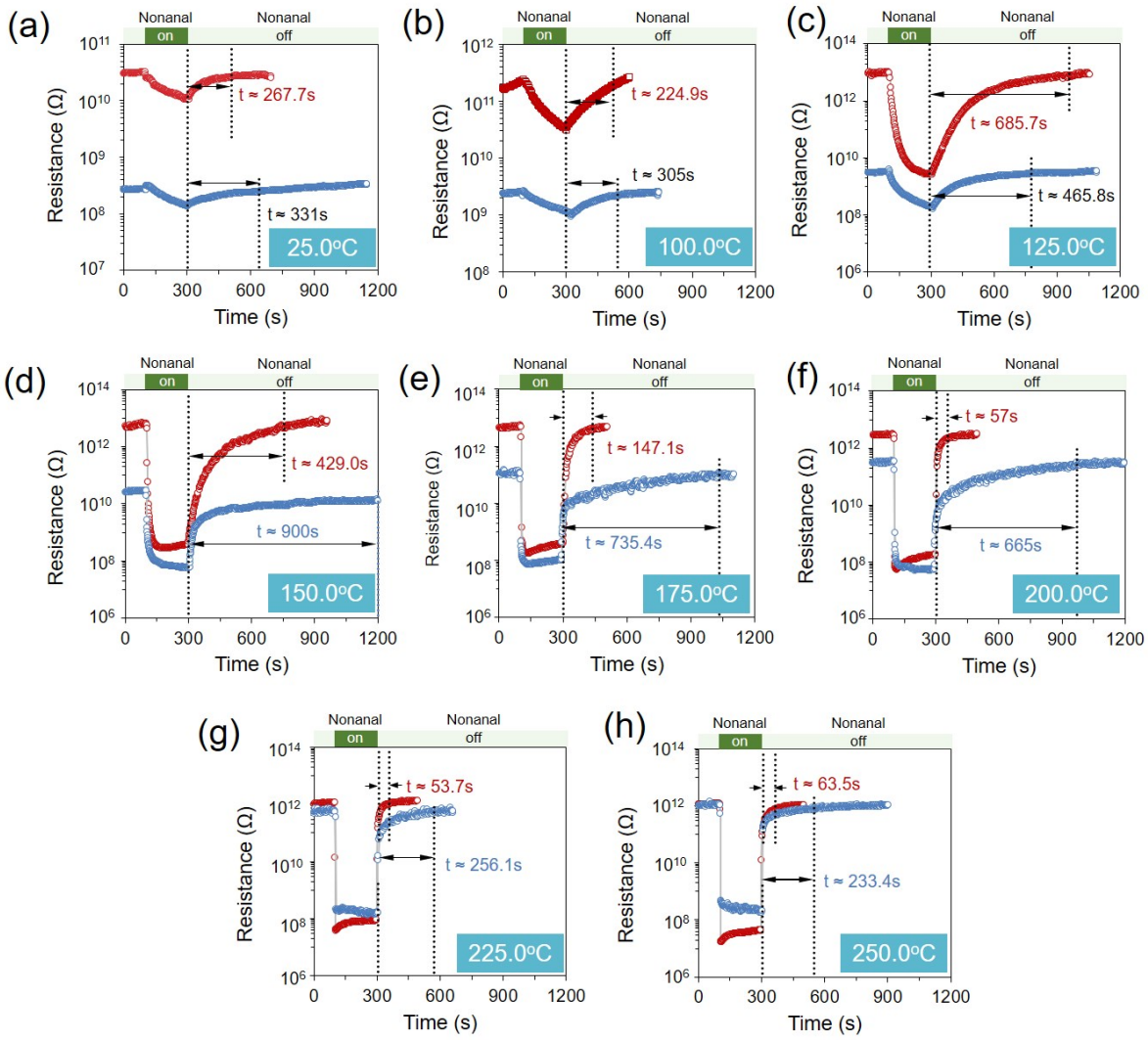


**Figure S3**. (a) – (f) Dynamic resistance response of *as-grown* and $H_2SO_4$-surface treated $WO_3$ nanowire sensor devices working at different temperatures (25 – 250 °C) to 2.67 ppm nonanal. (b) Sensing response and (j) recovery time extracted from (a) to (f).

**Table S1.** Summary of nonanal sensing performance in previous studies and this study.

| Sensor type | Material | Sensitivity ($R_{air/N2}/R_{gas}$) | Recovery time | Operation temperature | Ref. |
|---|---|---|---|---|---|
| Metal oxide semiconductor sensor | Pt, Pd, Au/$SnO_2$ | ~5 (55 ppb) | 102 s | 250 °C | 4 |
| | Pt, Pd, Au/$SnO_2$ nanoparticles/nanosheet | ~3 (55 ppb) | 102 s | 300 °C | 5 |
| | Pt, Pd, Au/$SnO_2$ nanoparticles/nanosheet | ~10-20 (55 ppb) | several to tens of minutes | 250 °C | 6 |
| | $SnO_2$ nanosheet | ~1.38 (100 ppb) | - | 250 °C | 7 |
| | $WO_3$ nanowires textile | 2.96 (2.7ppm) | 66 s | RT | 8 |
| | Single $WO_3$ nanowire | 3.80 (27ppb) | 252 s | 200 °C | 9 |
| | **Single $WO_3$ nanowire (Acid surface treatment)** | **58 (6.67ppb)** | **48.4 s** | **200 °C** | **This work** |
| | | **$10^4$-$10^5$ (2.7ppm)** | **>200 s** | **200 °C** | |
| Chemiresistive sensor | Molecularly functionalized gold nanoparticles | 190ppb | – | RT | 10 |
| | Polymer and carbon black | 3.42 ppm | – | Unknown | 11 |
| | Molecularly functionalized gold nanoparticles | 50 ppb | – | Unknown | 12 |
| Field effect transistor | DNA-decorated carbon nanotubes | 0.1% of saturated vapor | – | RT | 13 |
| QCM | Molecularly imprinted $TiO_2$ | Several ppm | >1800 s | RT | 14 |

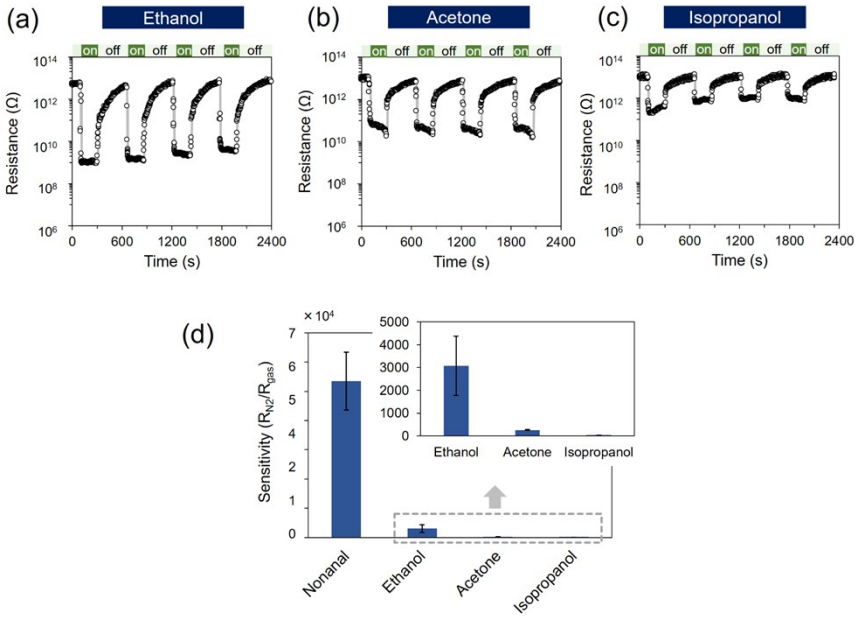


**Figure S4.** (a)-(c) Dynamic resistance response of $H_2SO_4$-surface treated $WO_3$ nanowire sensor device to various volatile molecules (nonanal (2.67 ppm), ethanol (~11.8 ppm), acetone (~48.5 ppm), isopropanol (~8.7 ppm)). (d) Sensitivity of $H_2SO_4$-surface treated $WO_3$ nanowire sensor device to various volatile molecules that extracted from (a)-(c). Inset shows the magnified data for ethanol, acetone and isopropanol. The sensing measurements are performed at 200 ºC with the readout voltage of 1 V under $N_2$ flow in air.

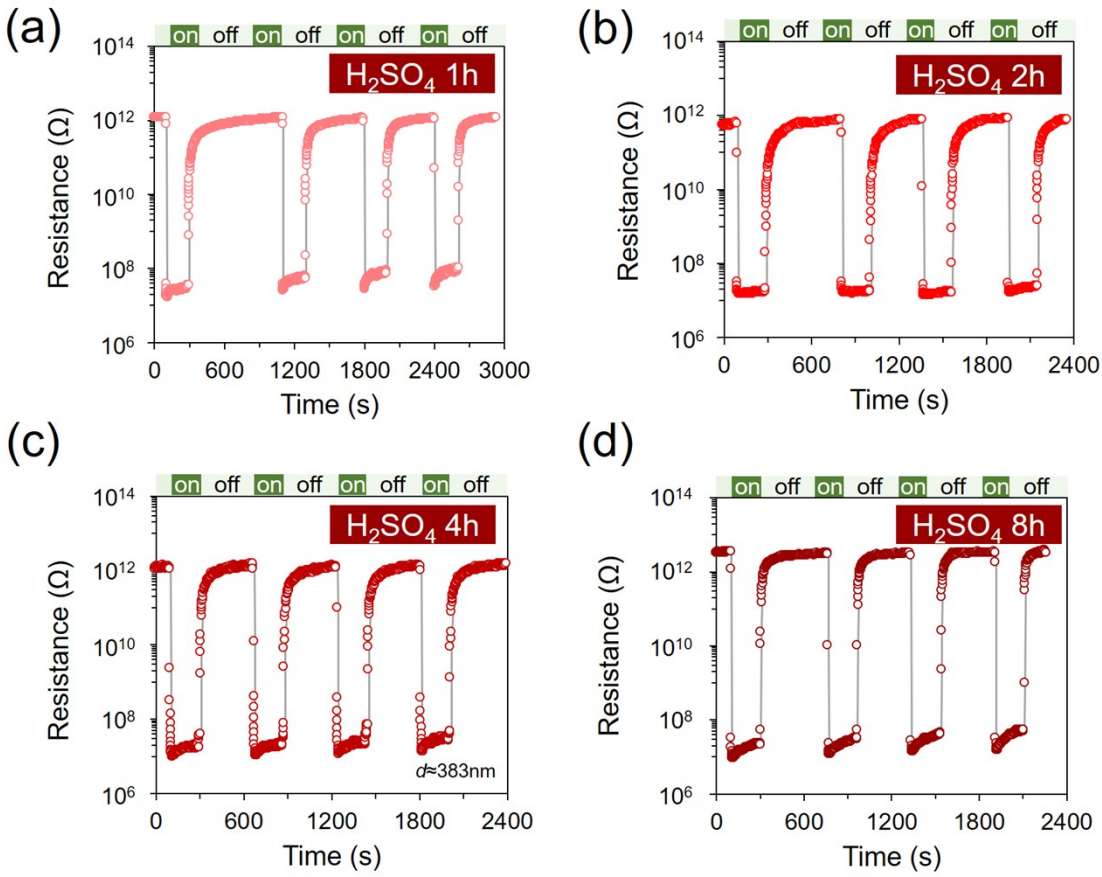


**Figure S5**. (a) – (d) Dynamic resistance response of different time (1 – 8 h) treated $WO_3$ nanowire sensor devices to 2.67 ppm nonanal at 200 $^{o}$C.

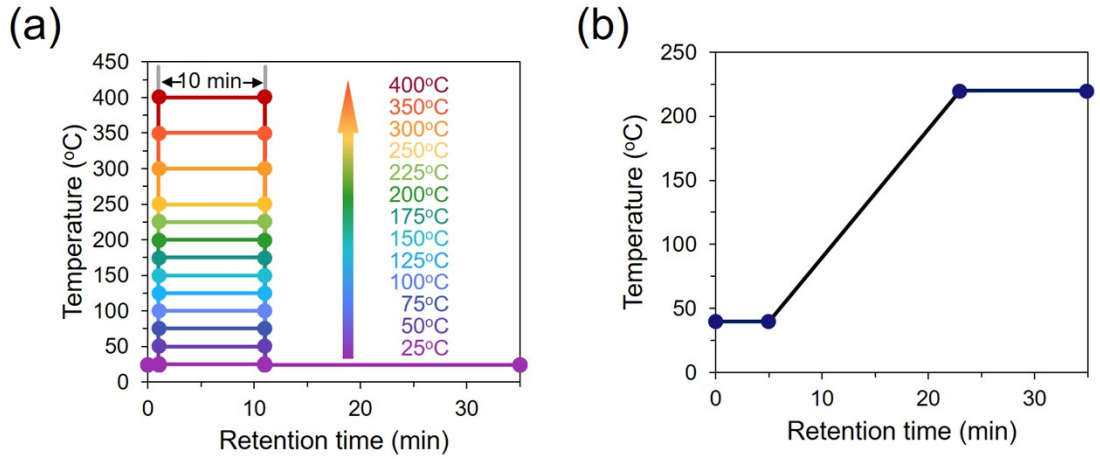


**Figure S6.** The temperature program for desorbed gas analysis by GC-MS: (a) Inlet temperature; (b) Column temperature.

The inlet temperature and column temperature were controlled with the program shown in Figure S5. The inlet temperature programs were sequentially executed for the condition of 25 °C, 50 °C, 75 °C, 100 °C, 125 °C, 150 °C, 175 °C, 200 °C, 225 °C, 250 °C, 300 °C, 350 °C and 400. The same column temperature program (Figure S5b) was used for each inlet-temperature condition.

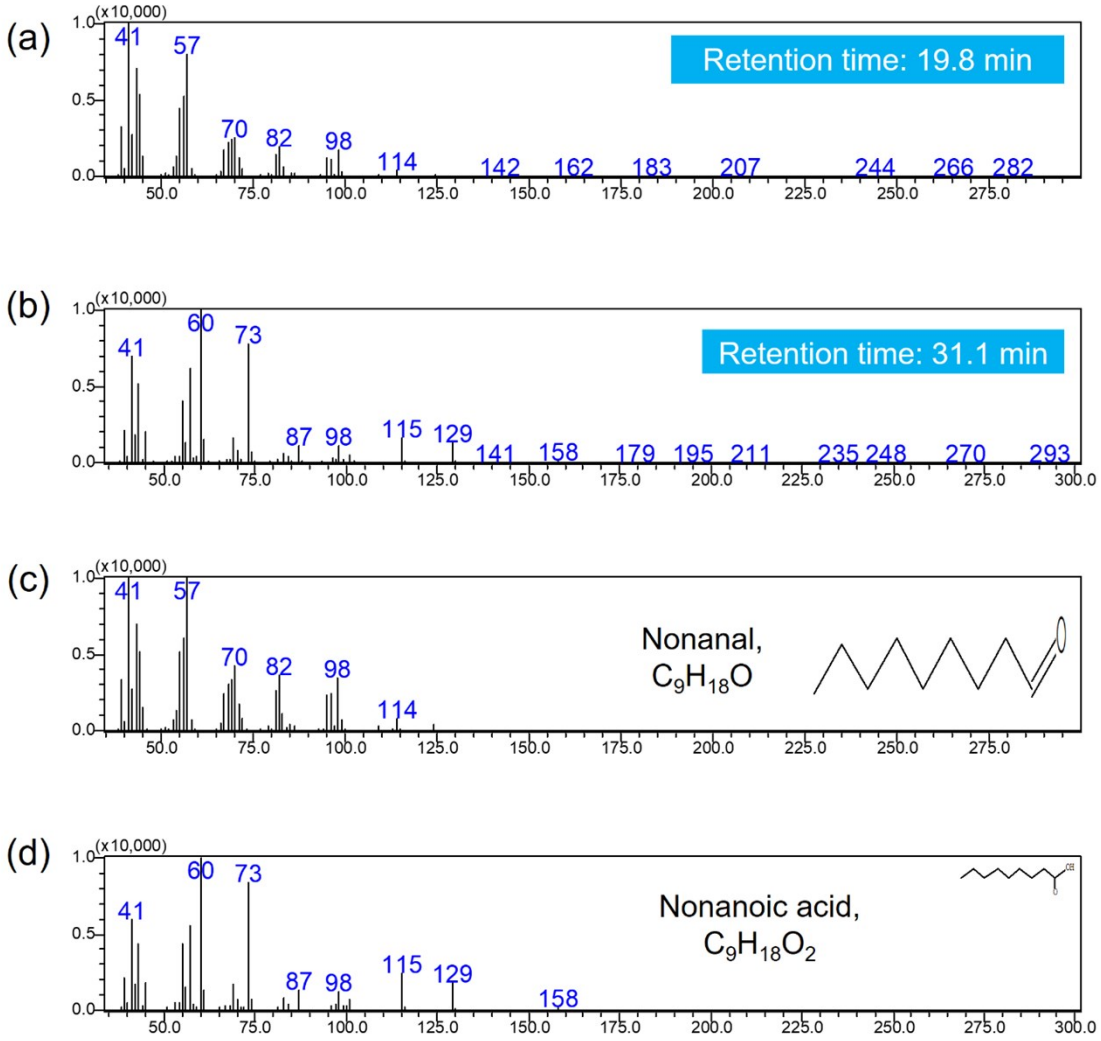


**Figure S7** The MS fragment pattern of the desorbed molecules from the nonanal-adsorbed $WO_3$ nanowire (*as-grown* and $H_2SO_4$-surface treated) at (a) retention time: 19.8 min and (b) retention time: 31.1 min. The library MS pattern of (c) nonanal and (d) nonanoic acid.

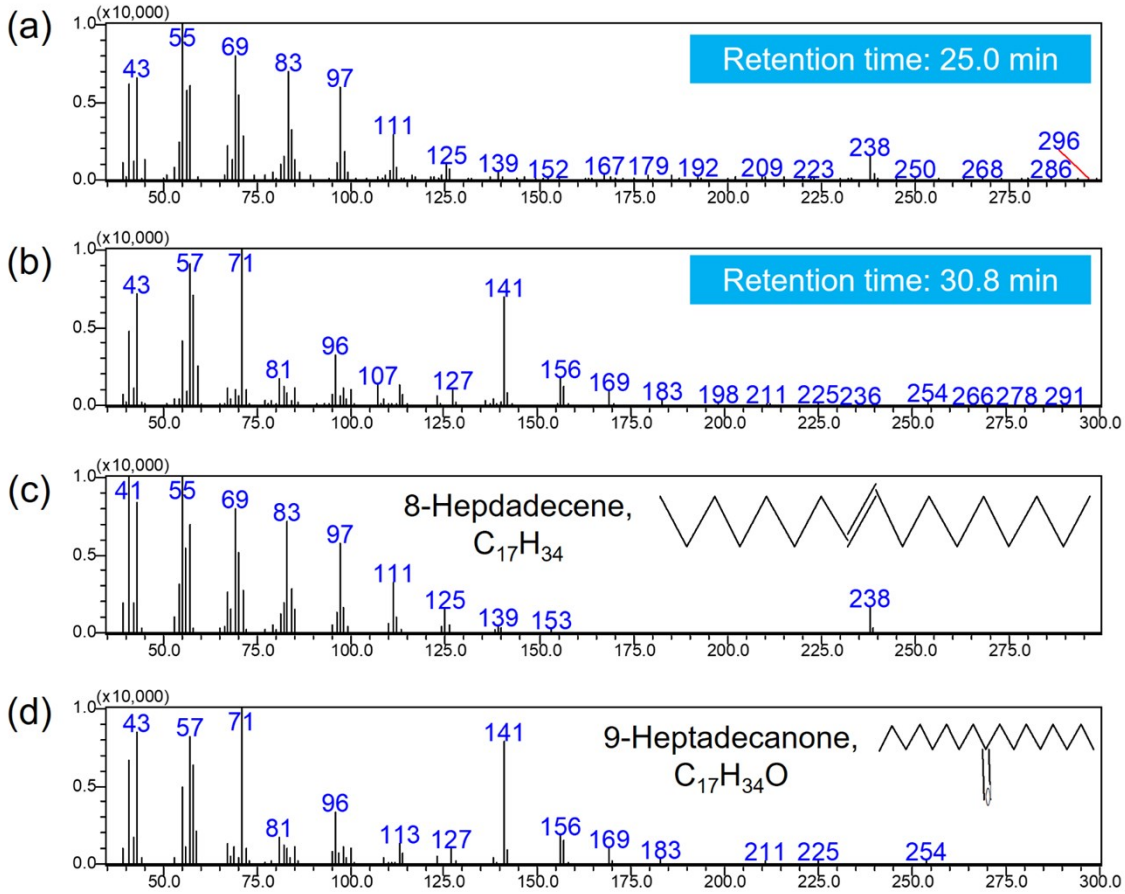


**Figure S8**. The MS fragment pattern of the desorbed molecules from the nonanal-adsorbed $WO_3$ nanowire (*as-grown*) at (a) retention time: 25.0 min and (b) retention time: 30.8 min above 200$^{o}$C heating. The library MS pattern of (c) 1-Hexadecene and (d) 9-Heptadecanone.

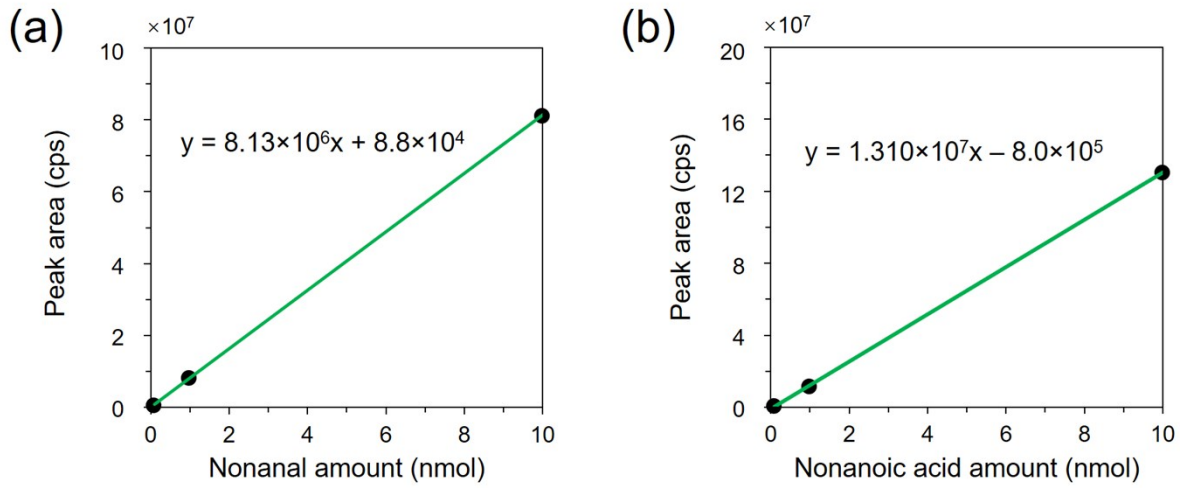


**Figure S9**. (a) Nonanal and (b) nonanoic acid concentration calibration by GC-MS.

## Computational analyses of molecular vibrational infrared spectra

We simulated the infrared spectra of nonanal adsorptions on the $W^{6+}$ site using density functional theory (DFT). A cluster model was used to model the hexagonal $WO_3$ (100) surface. The cluster model for the $W^{6+}$ site model consisted of a single tungsten atom and five oxygen atoms. Each oxygen atoms were passivated by a hydrogen atom. Such a capping hydrogen atom was positioned 0.96 Å along each a chemical bond between each oxygen atom and the nearest tungsten atom which was not included in the cluster model. We fixed the atomic configurations of these two cluster models during the geometry optimizations. The vibrational harmonic frequency calculations were performed not in the whole systems but in these partially optimized systems. We employed four different functionals ( $\omega$B97XD, APFD, B3LYP, B3LYP-D3) with the def2-SVP basis sets. The Becke and Johnson's damping function was used with B3LYP-D3. All the DFT calculations were performed by the Gaussian program package Revision A 03.

Figure S9 shows the obtained infrared spectrum, where the vibrational frequencies are scaled by 0.97 in order to consider the anharmonic effects effectively.

The characteristic frequency of C=O stretching (str.) at the $W^{6+}$ site was computed to be 1687.7, 1682.2, 1657.1, and 1658 $cm^{-1}$ with $\omega$B97XD, APFD, B3LYP, and B3LYP-D3, respectively. The small difference between the B3LYP-D3 and B3LYP functionals shows the dispersion force is not crucial to explain the interactions between nonanal's C=O and the $W^{6+}$ site. On the basis of the harmonic frequency calculations, we assigned the experimentally observed peak at 1668 $cm^{-1}$ to C=O str. on the $W^{6+}$ site.

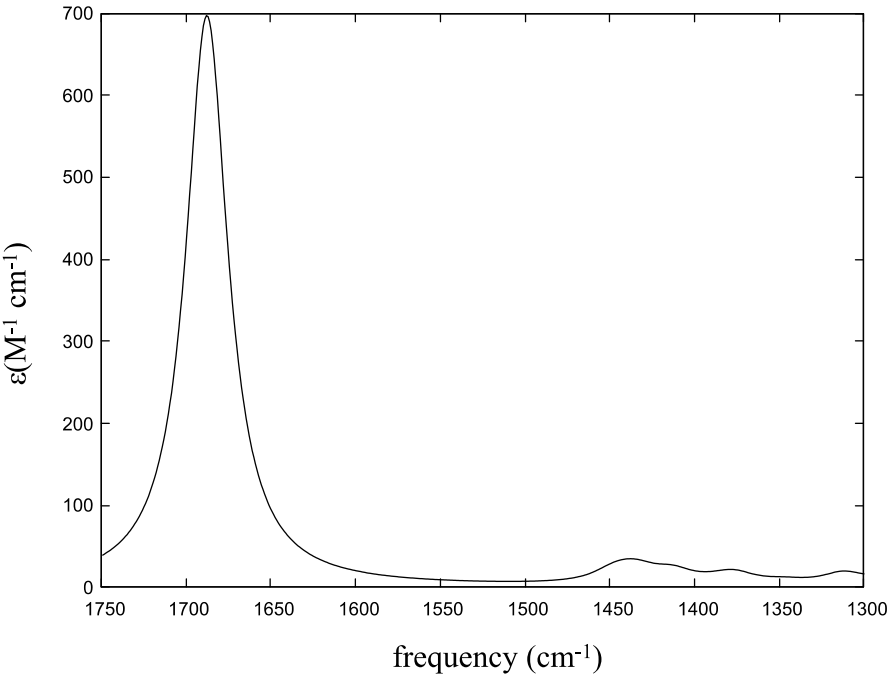


**Figure S10**. Simulated infrared spectra of nonanal adsorbed on the $W^{6+}$ site. The computational level is $\omega$B97XD/def2-SVP. The scaling factor 0.97 was employed.

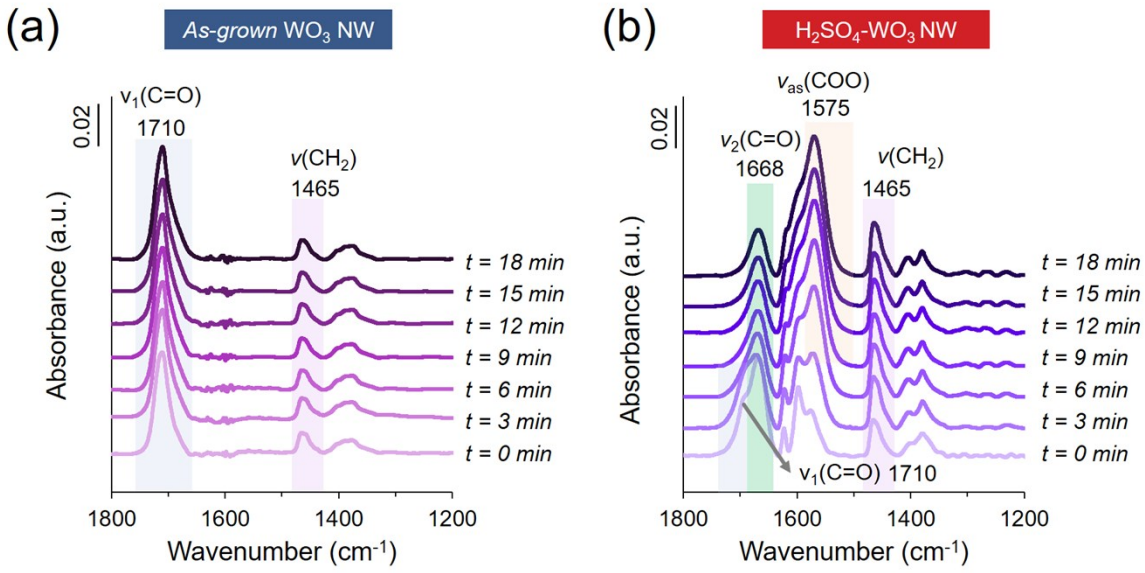


**Figure S11**. (a) and (b) are time-dependent FTIR spectra during the diffusion process of nonanal molecules adsorbed on *as-grown* $WO_3$ hydrate nanowires and $H_2SO_4$-surface treated $WO_3$ hydrate nanowires surface. (Measurement temperature, 25°C)

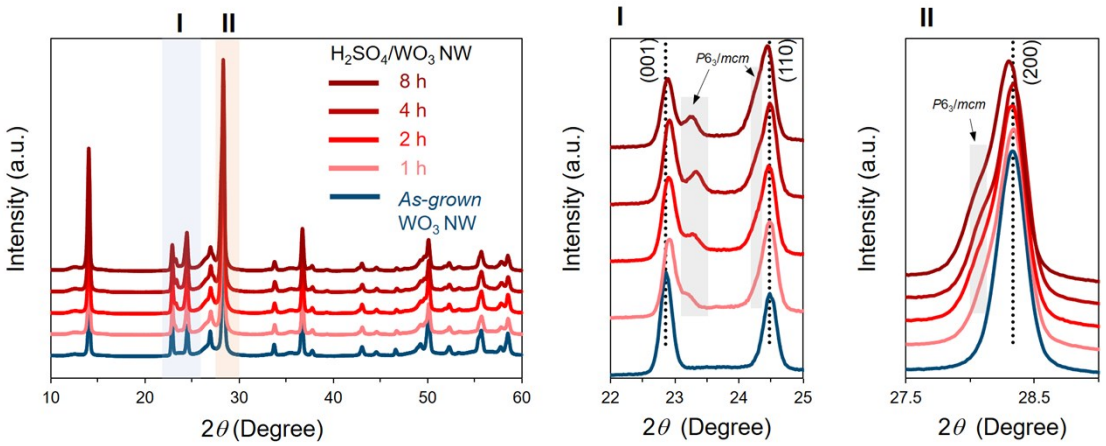


**Figure S12**. XRD patterns of *as-grown* and $H_2SO_4$-surface treated $WO_3$ hydrate nanowire samples.

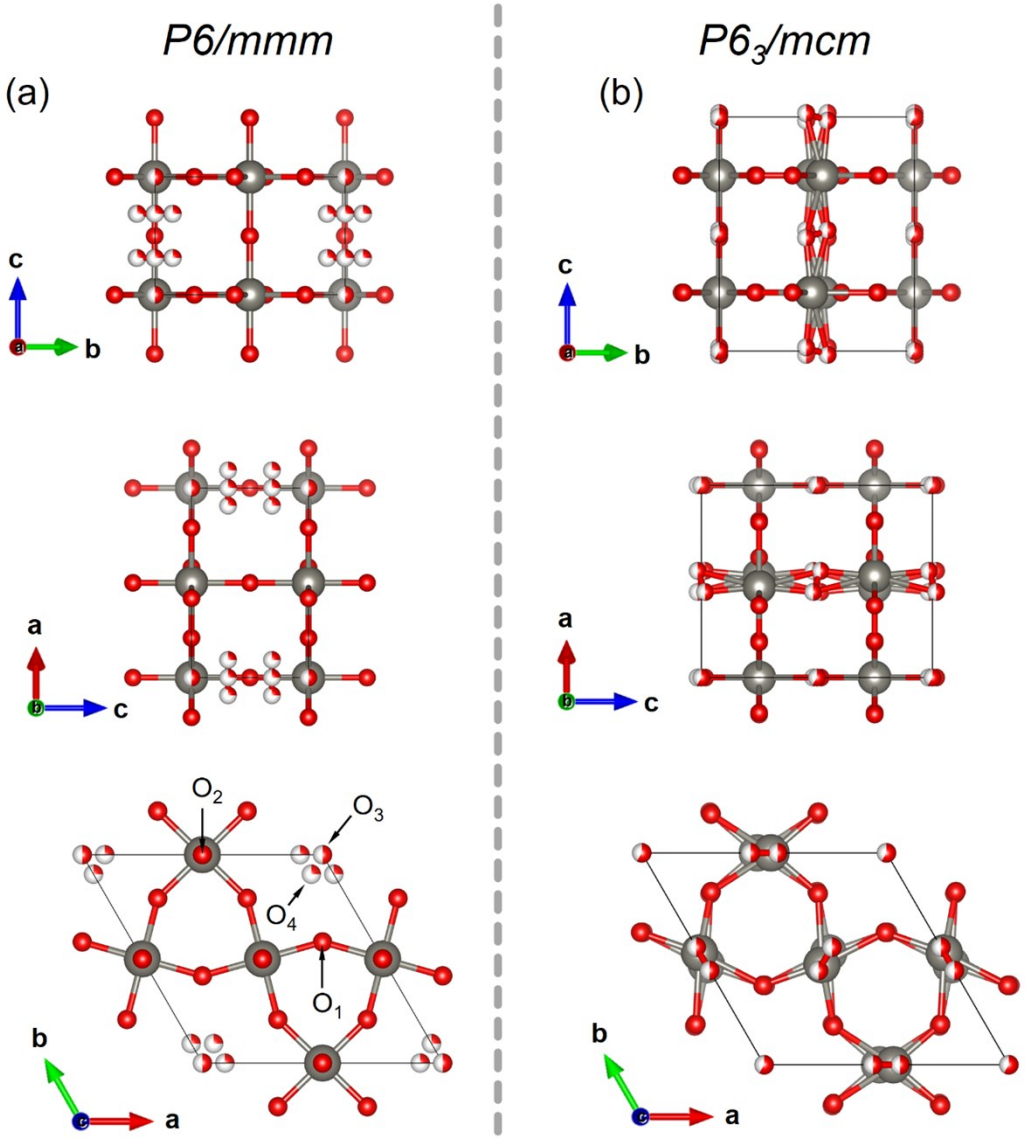


**Figure S13**. The refined crystal structure of hexagonal tungsten hydrates with (a) *P6/mmm* (as-grown nanowire) and (b) *P6$_3$/mcm* ($H_2SO_4$-surface treated nanowire) space group, viewed along *a*, *b* and *c* ($O_3$ oxygen is positioned in the center of the dodecagon aligned with the tungsten, while $O_4$ oxygen offsets from the tungsten in the *c* axis slightly towards the $O_2$ oxygen. The red sectors in water "dots" represent the probability of water's presence at the corresponding sites.

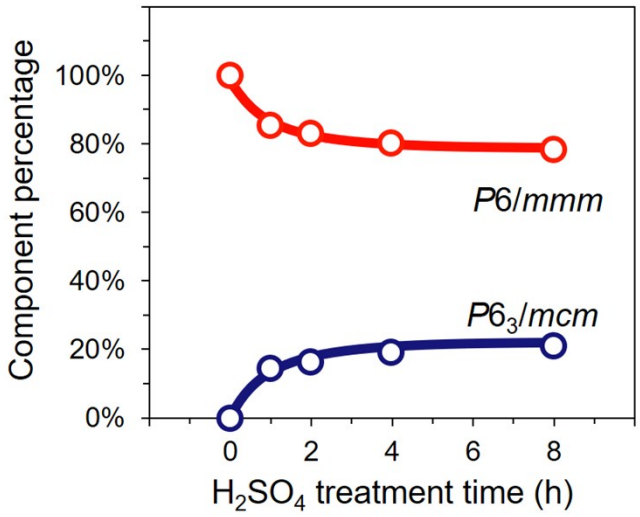


**Figure S14**. The structure percentage of hexagonal $WO_3$ hydrate nanowire that varied with the $H_2SO_4$-surface treatment time. These data are calculated from the Rietveld refinement of X-ray diffraction (XRD) patterns.

**Table S2** Results of the refinement data of *as-grown* $WO_3$ hydrate nanowire in the Space Group P6/mmm

| Space Group | | Atom | x | y | z | Occupancy | Site | Symmetry |
|---|---|---|---|---|---|---|---|---|
| *P6/mmm* (100%) | 1 | $W_1$ | 0.50000 | 0.00000 | 0.00000 | 1.00000 | 3f | mmm |
| | 2 | $O_1$ | 0.50000 | 0.00000 | 0.50000 | 1.00000 | 6l | mm2 |
| | 3 | $O_2$ | 0.20929 | 0.41865 | 0.00000 | 1.00000 | 3g | mmm |
| | 4 | $O_3$ | 0.00000 | 0.00000 | 0.00000 | 0.51840 | 1a | 6/mmm |
| | 5 | $O_4$ | 0.09350 | 0.09350 | 0.31256 | 0.25144 | 12n | ..m |

**Table S3** Results of the refinement data of $H_2SO_4$-surface treated (4h) $WO_3$ hydrate nanowire

| Space Group | | Atom | x | y | z | Occupancy | Site | Symmetry |
|---|---|---|---|---|---|---|---|---|
| *P6/mmm* (79.6%) | 1 | $W_1$ | 0.50000 | 0.00000 | 0.00000 | 1.00000 | 3f | mmm |
| | 2 | $O_1$ | 0.50000 | 0.00000 | 0.50000 | 1.00000 | 6l | mm2 |
| | 3 | $O_2$ | 0.20929 | 0.41865 | 0.00000 | 1.00000 | 3g | mmm |
| | 4 | $O_3$ | 0.00000 | 0.00000 | 0.00000 | 0.51840 | 1a | 6/mmm |
| | 5 | $O_4$ | 0.09350 | 0.09350 | 0.31256 | 0.25144 | 12n | ..m |
| *P6₃/mcm* (20.4%) | 1 | $W_1$ | 0.00000 | 0.47200 | 0.250000 | 1.00000 | 3f | mmm |
| | 2 | $O_1$ | 0.18300 | 0.37500 | 0.75000 | 1.00000 | 6l | mm2 |
| | 3 | $O_2$ | 0.00000 | 0.44500 | 0.01600 | 0.50000 | 3g | mmm |
| | 4 | $O_3$ | 0.00000 | 0.00000 | 0.00000 | 0.59856 | 1a | 6/mmm |
| | 5 | $O_4$ | 0.09350 | 0.09350 | 0.31256 | -0.30000 | 12n | ..m |

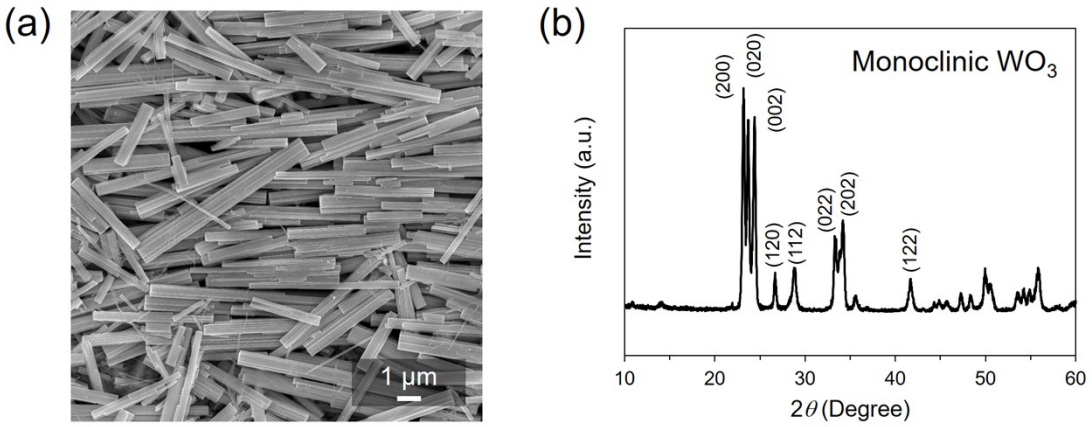


**Figure S15**. (a) SEM image and (b) XRD patterns of *as-grown* $WO_3$ hydrate nanowire after thermal annealing treatment (400$^{o}$C) for 1h.

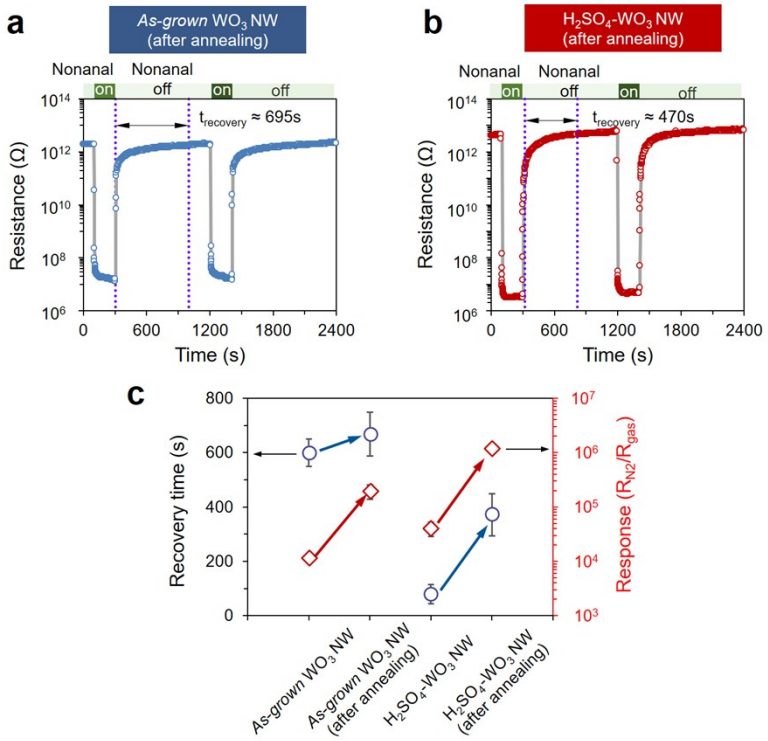


**Figure S16**. (a) and (b) are dynamic resistance response of the 400 °C annealed *as-grown* and $H_2SO_4$-surface treated $WO_3$ hydrate nanowire sensor devices to 2.67 ppm of nonanal under alternating flow of pure $N_2$ and nonanal bubbling gas at 200 °C. (c) Recovery time and sensing response of 400 °C annealing treated *as-grown* $WO_3$ hydrate and $H_2SO_4$-surface treated $WO_3$ hydrate nanowire devices at 200 °C.

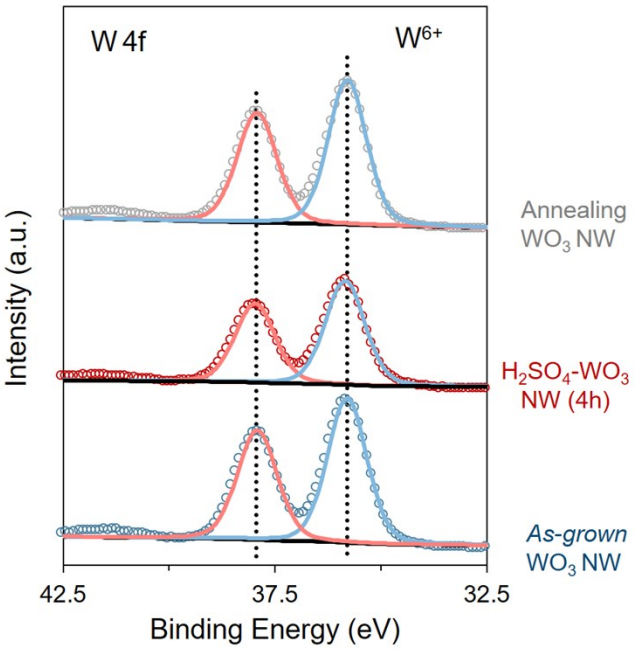


**Figure S17**. XPS W 4f spectra of as-grown $WO_3$ hydrate nanowire, $H_2SO_4$-surface treated (4 h) $WO_3$ nanowire and thermal annealing treated (400$^{o}$C air, 1 h) $WO_3$ hydrate nanowire.

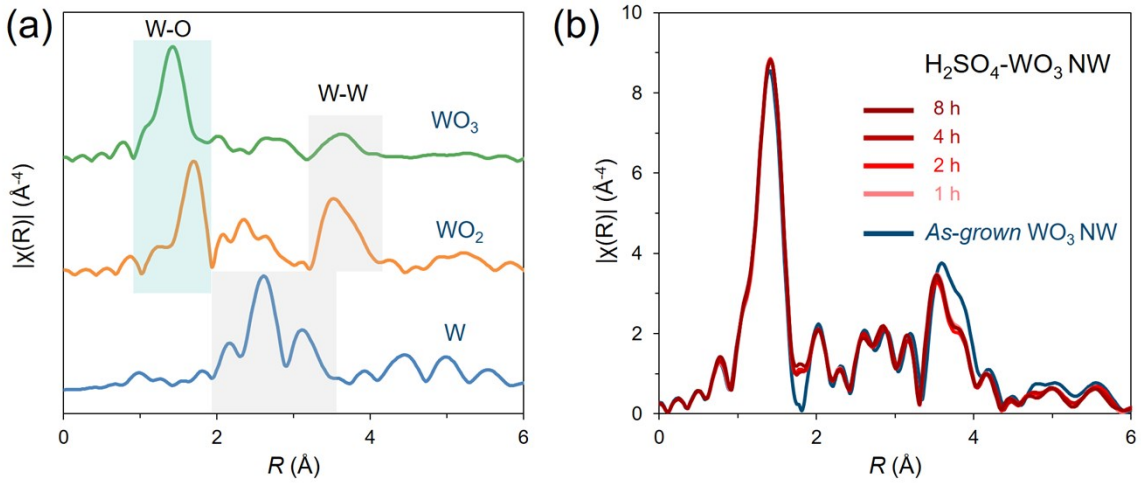


**Figure S18**. (a) Fourier transformed $k^3$-weighted χ(k)-function of the EXAFS spectra of standard W, $WO_2$ and $WO_3$ powder samples. (a) Fourier transformed $k^3$-weighted χ(k)-function of the EXAFS spectra of as-grown and $H_2SO_4$-surface treated $WO_3$ hydrate nanowire samples.

**Table S4.** EXAFS fitting parameters at the W L-edge various samples（$S_0^2$=0.67）

| Sample | Path | [a]C.N. | [b]$R$ (Å) | [c]$\sigma^2\times10^3$ (Å$^2$) | [d]$\Delta E_0$ (eV) | R factor |
|---|---|---|---|---|---|---|
| W std | W-W | 8* | 2.74±0.01 | 2.6±1.7 | 12.0±1.1 | 0.001 |
| | W-W | 6* | 3.15±0.01 | 3.1±0.2 | 11.0±2.0 | |
| *As-grown* $WO_3$ NW | W-$O_1$ | 3.96±0.34 | 1.77±0.01 | 4.3±1.2 | 5.6±2.0 | 0.007 |
| [e]TA_$WO_3$ NW | W-$O_1$ | 4.01±0.57 | 1.76±0.01 | 4.0±1.6 | 5.6±2.5 | 0.009 |
| [f]S_$WO_3$ NW (1h) | W-$O_1$ | 3.42±0.26 | 1.76±0.02 | 3.4±1.8 | 4.9±2.8 | 0.015 |
| S_$WO_3$ NW (2h) | W-$O_1$ | 3.45±0.26 | 1.76±0.02 | 3.6±1.9 | 4.8±2.8 | 0.009 |
| S_$WO_3$ NW (4h) | W-$O_1$ | 3.48±0.29 | 1.76±0.02 | 3.6±1.9 | 5.0±2.8 | 0.008 |
| S_$WO_3$ NW (8h) | W-$O_1$ | 3.42±0.34 | 1.76±0.02 | 3.5±2.0 | 4.8±3.0 | 0.010 |

[a]C.N.: coordination numbers; [b]$R$: bond distance; [c]$\sigma^2$: Debye-Waller factors; [d]$\Delta E_0$: the inner potential correction; [a]TA: Thermal annealing treatment (Air, 400$^o$C, 1h); [f]S: $H_2SO_4$-surface treatment. $R$ factor: goodness of fit. * the experimental EXAFS fit of standard W powder by fixing C.N. as the known crystallographic value.

The obtained XAFS data was processed in Athena (version 0.9.25) for background, pre-edge line and post-edge line calibrations. Then Fourier transformed fitting was carried out in Artemis (version 0.9.25). The $k^3$ weighting, k-range of 3 - 15 Å$^{-1}$ and R range of 1 - 1.72 Å for 1 shell were used for the fitting. The model of bulk W and $WO_3$ were used to calculate the simulated scattering paths. The four parameters, coordination number, bond length, Debye-Waller factor and $E_0$ shift (CN, $R$, $\sigma^2$, $\Delta E_0$) were fitted without anyone was fixed, constrained, or correlated.

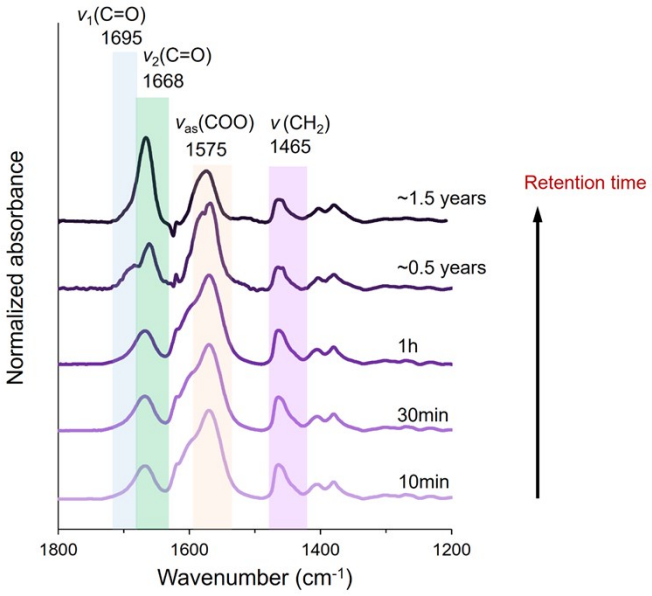


**Figure S19**. Retention time dependence of FT-IR spectra of $H_2SO_4$ surface treated $WO_3$ hydrate nanowire catalysis (without thermal annealing treatment).

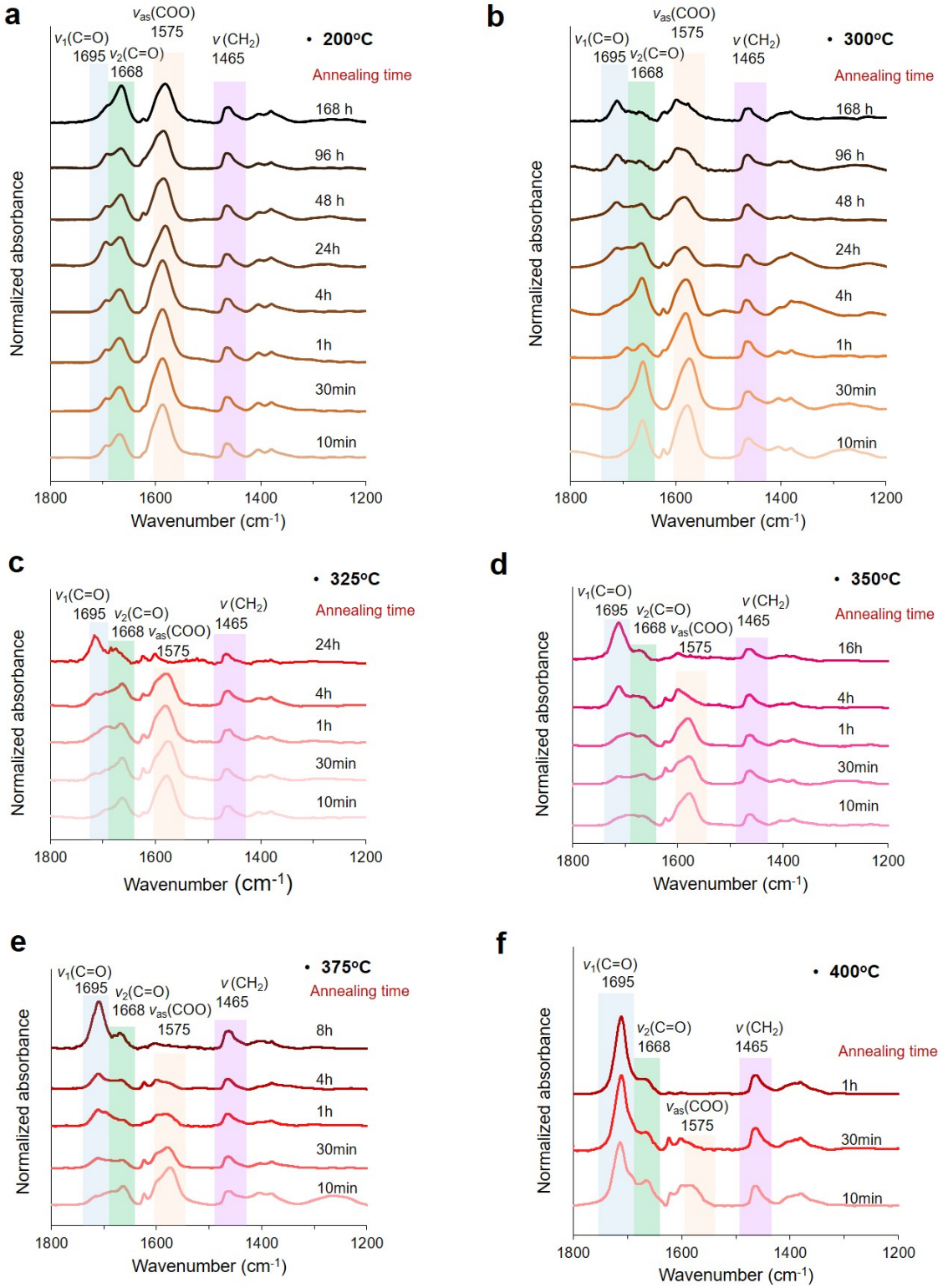


**Figure S20**. Annealing time dependence of FT-IR spectra of $H_2SO_4$ surface treated $WO_3$ hydrate nanowire catalysis after thermal annealing at (a) 200°C, (b) 300°C, (c) 325°C, (d) 350°C, (e) 375°C and (f) 400°C.

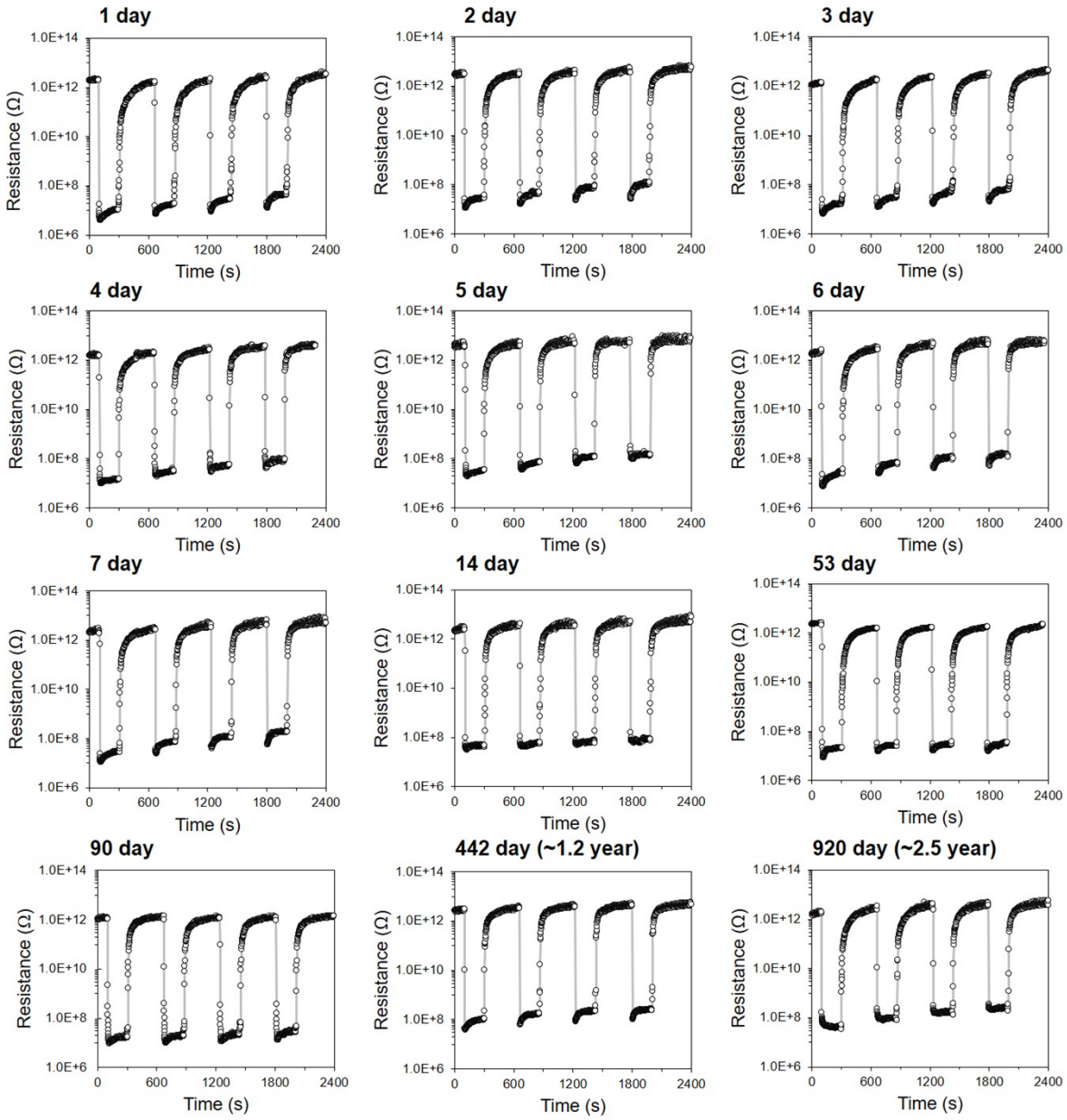


**Figure S21**. Long-term stability of $H_2SO_4$ surface treated $WO_3$ hydrate nanowire sensor device (working at 200°C, nonanal, 2.67ppm).

## References


1. Zhang, D. et al. Detection of $NO_2$ down to ppb levels using individual and multiple $In_2O_3$ nanowire devices. *Nano Lett.* **2004**, 4, 1919–1924.
2. Abbas, A. N. et al. Patterning, characterization and chemical sensing applications of graphene nanoribbon arrays down to 5 nm using helium ion beam lithography. *ACS Nano* **2014**, 8, 1538–1546.
3. Liu, B. et al. High-performance chemical sensing using schottky-contacted chemical Vapor deposition grown monolayer $MoS_2$ transistors. *ACS Nano* **2014**, 8, 5304–5314.
4. Itoh, T.; Miwa, T.; Tsuruta, A.; Akamatsu, T.; Izu, N.; Shin, W.; Park, J.; Hida, T.; Eda, T.; Setoguchi, Y. Development of an Exhaled Breath Monitoring System with Semiconductive Gas Sensors, a Gas Condenser Unit, and Gas Chromatograph Columns. *Sensors* **2016**, *16*, 1891
5. Itoh, T.; Nakashima, T.; Akamatsu, T.; Izu, N.; Shin, W. Nonanal gas sensing properties of platinum, palladium, and gold-loaded tin oxide VOCs sensors. *Sens. Actuators, B* **2013**, *187*, 135– 141
6. Masuda, Y.; Itoh, T.; Shin, W.; Kato, K. $SnO_2$ Nanosheet/Nanoparticle Detector for the Sensing of 1-Nonanal Gas Produced by Lung Cancer. *Sci. Rep.* **2015**, *5*, 1012
7. Masuda, Y.; Kato, K.; Kida, M.; Otsuka, J. Selective nonanal molecular recognition with $SnO_2$ nanosheets for lung cancer sensor. *Int. J. Appl. Ceram. Technol.* **2019**, *16*, 1807– 1811,
8. Zhang, G.; Wang, C.; Mizukami, W.; Hosomi, T.; Nagashima, K.; Yoshida, H.; Nakamura, K.; Takahashi, T.; Kanai, M.; Yasui, T.; Aoki, Y.; Baba, Y.; Yanagida, T. Monovalent sulfur oxoanions enable millimeter-long single-crystalline *h*-$WO_3$ nanowire synthesis. *Nanoscale* **2020**, *12*, 9058– 9066
9. Nekita, S., Nagashima, K., Zhang, G., Wang, Q., Kanai, M., Takahashi, T., ... & Yanagida, T. (2020). Face-Selective Crystal Growth of Hydrothermal Tungsten Oxide Nanowires for Sensing Volatile Molecules. *ACS Applied Nano Materials*, *3*(10), 10252-10260.
10. Jin, H.; Huynh, T.-P.; Haick, H. Self-Healable Sensors Based Nanoparticles for Detecting Physiological Markers via Skin and Breath: Toward Disease Prevention via Wearable Devices. *Nano Lett.* **2016**, *16*, 4194– 4202
11. Huynh, T.-P.; Khatib, M.; Srour, R.; Plotkin, M.; Wu, W.; Vishinkin, R.; Nayek, N.; Jin, H.; Gazit, O. M.; Haick, H. Composites of Polymer and Carbon Nanostructures for Self-Healing Chemical Sensors. *Adv. Mater. Technol.* **2016**, *1*, 1600187

12. Kahn, N.; Lavie, O.; Paz, M.; Segav, Y.; Haick, H. Dynamic Nanoparticle-Based Flexible Sensors: Diagnosis of Ovarian Carcinoma from Exhaled Breath. *Nano Lett.* **2015**, *15*, 7023– 7028
13. Khamis, S. M.; Jones, R. A.; Johnson, A. T. C.; Preti, G.; Kwak, J.; Gelperin, A. DNA-decorated carbon nanotube-based FETs as ultrasensitive chemical sensors: Discrimination of homologues, structural isomers, and optical isomers. *AIP Adv.* **2012**, *2*, 022110
14. Liu, C.; Wyszynski, B.; Yatabe, R.; Hayashi, K.; Toko, K. Molecularly Imprinted Sol-Gel-Based QCM Sensor Arrays for the Detection and Recognition of Volatile Aldehydes. *Sensors* **2017**, *17*, 382.